Modeling of the temperature-dependent spectral response of $In_{1-\chi}Ga_{\chi}Sb$ infrared photodetectors.

Juan A. González-Cuevas
Department of Electrical and Computer Engineering
Old Dominion University
Norfolk, VA, 23529

Tamer F. Refaat
Science and Technology Corporation
NASA Langley Research Center
Hampton, VA 23681

M. Nurul Abedin
Passive Sensor Systems Branch
NASA Langley Research Center
Hampton, VA 23681

Hani E. Elsayed-Ali
Department of Electrical and Computer Engineering
Old Dominion University
Norfolk, VA, 23529

Modeling of the temperature-dependent spectral response of $In_{1-\chi}Ga_{\chi}Sb$ infrared photodetectors.

Abstract

A model of the spectral responsivity of $In_{1-\chi}Ga_{\chi}Sb$ p-n junction infrared photodetectors has been developed. This model is based on calculations of the photogenerated and diffusion currents in the device. Expressions for the carrier mobilities, absorption coefficient and normal-incidence reflectivity as a function of temperature were derived from extensions made to Adachi and Caughey-Thomas models. Contributions from the Auger recombination mechanism, which increase with a rise in temperature, have also been considered. The responsivity was evaluated for different doping levels, diffusion depths, operating temperatures, and photon energies. Parameters calculated from the model were compared with available experimental data, and good agreement was obtained. These theoretical calculations help to better understand the electro-optical behavior of $In_{1-\chi}Ga_{\chi}Sb$ photodetectors, and can be utilized for performance enhancement through optimization of the device structure.

Keywords: Photodetectors, Spectral Response, Temperature Effect, Optical Properties, Electrical Properties, InGaSb

1. INTRODUCTION

The spectral response is an important characteristic for defining the performance of a photodetector. This characteristic specifies the responsivity, defined as the generated photocurrent per unit optical power, variation with wavelength. The photodetector responsivity is primarily dependent on the device material, structure and the operating conditions in terms of bias voltage, temperature, and wavelength of the incident radiation. It thus becomes crucial to have a thorough understanding of the effects of these parameters in order to design and fabricate an optimal photodetector. A theoretical model for the spectral response is particularly useful to accomplish such task.

Antimonide based ternary III-V compounds are good materials for photodetectors operating in the infrared range. These devices have several applications such as atmospheric remote sensing, hazardous gas detection, and optical fiber communication[1]. InGaSb ternary alloy systems show a promising performance in the 1.7 to 5-μm wavelength range. By varying the indium composition, the detection wavelength could be tuned to optimize the quantum efficiency. Epitaxial growth of InGaSb on different binary substrates has been reported using different techniques[2]. Besides the complexity of these techniques, tuning to a specific wavelength usually involves performance deterioration mainly due to lattice mismatch problems. Lattice mismatch increases dark current and noise, limiting both dynamic range and sensitivity of a detector. The availability of bulk ternary substrates significantly simplifies the fabrication process by using simpler and lower cost techniques.[3]

In this paper, a model is developed for the responsivity of $In_{1-\chi}Ga_{\chi}Sb$ p-n photodetectors. The model includes the temperature effects on the various parameters and their influence on the spectral response of the device. Also the significance of using a ternary substrate will be presented. The

model is based on studying the excess minority carrier generation, recombination and diffusion by applying the continuity equations.

The device responsivity, and therefore quantum efficiency, is affected by the absorption coefficient, reflection coefficient and minority carriers recombination lifetimes. The absorption and reflection coefficients are calculated using Adachi's model,[4-8] modified to include temperature effects. The mobility is calculated using an extended Caughey-Thomas model,[9-11] which accounts for both temperature and carrier concentration. The main mechanisms acting on the minority carriers lifetimes are the Shockley-Read-Hall (SRH) recombination,[12-14] and Auger recombination[15-19] besides the surface recombination effects. The Auger processes are strongly dependent on temperature at high concentrations and have a limiting effect on the device responsivity. Validation of the model is performed through comparison with experimental characterization of actual $In_{0.2}Ga_{0.8}Sb$ photodiodes. These photodiodes were manufactured by simple diffusion technique, using an InGaSb ternary substrate.[20]

The paper is organized as follows; in section 2, the methodology is introduced for calculating the temperature dependency of the energy bands, optical dispersion relations, and the effects of mobility and recombination lifetime on diffusion length, all of which are required for determining the photocurrent densities and spectral responsivity using the continuity equations. In section 3, results obtained from the model are presented and discussed, giving emphasis to the variation of the responsivity with temperature and the influence of using the ternary substrate. Finally, conclusions are given in section 4.

2. METHODOLOGY

The modeling of the thermal characteristics of the spectral response is based on calculating the device parameters considering their relationship to the energy band structure of the material. The schematic for the modeled photodiode structure is shown in Fig. 1. These photodiodes were manufactured by Zn diffusion to form the p-layer on an n-type InGaSb ternary substrate.[20] The resulted photodetector has a p-n junction structure illuminated from the top p-layer. Considering a non-degenerated semiconductor with full ionization, the model assumes a steady-state solution, with low electric field not to saturate the carriers velocity.

2.1 Lattice parameters and energy bands

$In_{1-\chi}Ga_{\chi}Sb$ is a ternary alloy whose parameters and characteristics change according to its composition, χ. The lattice parameters for $In_{1-\chi}Ga_{\chi}Sb$ are obtained from the linear interpolation of the transition parameters of the binary materials InSb and GaSb using the relation[21]

$$Q_{alloy} = \chi . B_{GaSb} + (1-\chi) B_{InSb} - \chi(1-\chi) C_B , \quad (1)$$

where B and Q represent the binary and ternary parameters, respectively, and C_B is the bowing parameter that accounts for contributions arising from lattice disorders.[8,21]

Applying Eq. 1, the electron effective mass corresponding to the conduction band, m_e, heavy-hole band, m_h, and spin split-off band, m_{so}, as well as the relative permittivity, ε_s, for $In_{1-\chi}Ga_{\chi}Sb$, are given by $m_e = \left(0.015 + 0.01\chi + 0.025\chi^2\right) \cdot m_o$, $m_h = \left(0.43 - 0.03\chi\right) \cdot m_o$, $m_{so} = \left(0.19 + 0.05\chi\right) \cdot m_o$, and $\varepsilon_s = \left(16.8 - 1.1\chi\right) \cdot \varepsilon_o$, respectively, where m_o is the electron rest mass, and ε_o is the absolute permittivity.[22]

The energy bandgap, E, variation with temperature, T, due to the temperature-dependent dilation of the lattice and electron-lattice interaction, is approximated by the semi-empirical Varshni equation[23]

$$E(T) = E(0) - \frac{\delta T^2}{(T + \beta)}, \quad (2)$$

where $E(0)$ is the energy bandgap value at absolute zero, and δ and β are fitting constants. Table I lists GaSb and InSb fitting constants for the different critical-point energies. Parameters for E_o, E_1, $E_1+\Delta_1$, and E_2 were taken from reported experimental data,[23-25] while the $E_o+\Delta_o$ temperature dependency for InSb was assumed to be parallel to E_o[24, 25]. Generally, the energy bands present an almost linear temperature dependence, with gradual increase at lower temperatures. Once the temperature dependent critical-point energies are defined for the binary materials, eq. (1) is applied to find the corresponding ternary material energies and its temperature dependence, with C_B = 0.2 eV only for E_o.[8, 21]

2.2 Optical dispersion parameters

The optical properties of a semiconductor are described by the complex dielectric function $\varepsilon(\lambda,T) = \varepsilon_1(\lambda,T) + i \cdot \varepsilon_2(\lambda,T)$, at all photon energies hc/λ, where h is Plank's constant, c is the speed of light and λ is the radiation wavelength. The real and imaginary parts of the dielectric function, $\varepsilon_1(\lambda,T)$ and $\varepsilon_2(\lambda,T)$, respectively, are analytically related using the Kramers-Kronig relation. The imaginary part is calculated from the joint density of states function at various critical point energies in the Brillouin zone and indirect band-gap transitions, as shown by S. Adachi.[4-8] Thus, the complex dielectric function is strongly related to the energy-band structure of the medium and its temperature dependency. The parameters used in calculating the dielectric function of

$In_{1-\chi}Ga_{\chi}Sb$ have been interpolated from InSb and GaSb data using Eq. (1).[5] Cooling down the device shifts the dielectric function to higher energy corresponding to shorter wavelength, agreeing with reported data.[24,25] The absorption coefficient, $\alpha(\lambda,T)$, and reflection coefficient, $R(\lambda,T)$, can now be calculated using the relations[8]

$$\alpha(\lambda,T)=\frac{4\pi}{\lambda}\cdot\sqrt{\frac{\sqrt{\varepsilon_1(\lambda,T)^2+\varepsilon_2(\lambda,T)^2}-\varepsilon_1(\lambda,T)}{2}} \tag{3}$$

$$R(\lambda,T)=\frac{\sqrt{\varepsilon_1(\lambda,T)^2+\varepsilon_2(\lambda,T)^2}-\sqrt{2\varepsilon_1(\lambda,T)+2\sqrt{\varepsilon_1(\lambda,T)^2+\varepsilon_2(\lambda,T)^2}}+1}{\sqrt{\varepsilon_1(\lambda,T)^2+\varepsilon_2(\lambda,T)^2}+\sqrt{2\varepsilon_1(\lambda,T)+2\sqrt{\varepsilon_1(\lambda,T)^2+\varepsilon_2(\lambda,T)^2}}+1} \tag{4}$$

Fig. 2 shows the absorption and reflection coefficients for $In_{0.2}Ga_{0.8}Sb$ at temperatures of 253, 273 and 293 K within the wavelength range of interest to the device analysis.

Applying eqs (3) and (4), the minority carrier optical generation rate $G(x,\lambda,T)$ along the device depth (x- direction in Fig. 1) is given by applying Beer-Lambert's relation according to[26]

$$G(x,\lambda,T)=\frac{\lambda\cdot P_{opt}(\lambda)\cdot\alpha(\lambda,T)\cdot[1-R(\lambda,T)]}{h\cdot c\cdot exp[\alpha(\lambda,T)\cdot x]}, \tag{5}$$

where $P_{opt}(\lambda)$ is the total optical power incident on the photodetector per unit area.

2.3 Temperature dependence of the mobilities

The minority carrier mobilities can be determined by analyzing the scattering mechanisms due to the ionized impurities and absorption (or emission) of either acoustical or optical phonons. According to Mathiesen's rule, the mobility of the $In_{1-\chi}Ga_{\chi}Sb$ alloy is determined from its binary compound mobilities using Eq. (1), with inverse mobilities for parameters Q and B and no bowing effect.[27] Besides, under low field conditions, majority carrier Hall mobilities and minority carrier

drift mobilities are very close to each other[11]. Thus, the electron (n) and hole (p) mobilities for both InSb and GaSb were taken from existing Hall mobility data,[11,27-30] which was fitted to the temperature extended Caughey-Thomas empirical model for III-V compounds, described by[9,11]

$$\mu(N,T)_{<n,p>} = \mu_{min,<n,p>} + \frac{\mu_{max,<n,p>}\left(\frac{300}{T}\right)^{\theta_{1,<n,p>}} - \mu_{min,<n,p>}}{1+\left(\frac{N_{<A,D>}}{N_{ref,<n,p>}\left(\frac{T}{300}\right)^{\theta_{2,<n,p>}}}\right)^{\phi_{,<n,p>}}}, \quad (6)$$

where μ_{max} and μ_{min} are the carrier mobility values at low and high doping concentrations, respectively, N_{ref} is the reference doping concentration for which the mobility reduces to half the maximum value, and ϕ is a fitting parameter independent of temperature, for $T > 150$ K. The positive temperature coefficients θ_1 and θ_2 serve to accordingly reduce the lattice limited mobility μ_{max} and increase N_{ref} with a rise in temperature. Table II shows the parameters used in the extended Caughey-Thomas model to calculate Hall mobilities of electrons and holes for both GaSb and InSb.[10,11,27]

2.4 Minority carrier lifetimes

The minority carrier lifetime, τ, is comprised of a number of fundamental components owing to various recombination mechanisms. Considering the nonradiative Shockley-Read-Hall (τ_{SRH}) and Auger (τ_{Auger}) recombination lifetimes, the total minority carrier lifetime is obtained from the inverse of the sum of their reciprocals,[31] i.e., $\tau_{\langle n,p\rangle}^{-1} = \tau_{SRH,\langle n,p\rangle}^{-1} + \tau_{Auger,\langle n,p\rangle}^{-1}$.

The Shockley-Read–Hall trap-assisted recombination lifetime, caused by imperfections within the semiconductor, is expressed as[12,13]

$$\tau_{SRH,<n,p>} = \frac{1}{\sigma.N_t}\sqrt{\frac{m_{<e,h>}}{3k_BT}}, \tag{7}$$

where σ is the capture cross section of minority carriers and N_t is the density of traps, assigned the values of $1.5\text{x}10^{-19}$ m^2 and $1.17\text{x}10^{21}$ m^{-3}, respectively and k_B is the Boltzmann constant.[26]

Of the possible known Auger recombination mechanisms, the most important for InSb-based compounds are between the conduction/valence bands (A-1) and through the conduction/heavy-hole/light-hole bands (CHLH or A-7). In the case of $In_{0.2}Ga_{0.8}Sb$, the energy bands of the alloy tend towards a GaSb configuration, wherein the magnitude of the spin split-off gap Δ_0 is significant to the E_0 energy gap.[17,18] Then the Auger recombination through the conduction/heavy-hole/spin split-off bands (CHSH or A-S) becomes significant. Thus, the total Auger lifetime can be expressed as[18]

$$\frac{1}{\tau_{Auger,<n,p>}} = \frac{n_{<p0,n0>} + p_{<p0,n0>}}{2}\left[\frac{1}{p_{<p0,n0>}\tau^i_{A1}} + \frac{1}{n_{<p0,n0>}\tau^i_{A7}} + \frac{1}{n_{<p0,n0>}\tau^i_{AS}}\right]. \tag{8}$$

In the above equation, $n_{<p0,n0>}$ and $p_{<p0,n0>}$ are the electron and hole carrier concentrations at equilibrium, $\tau_{A1}{}^i$, $\tau_{A7}{}^i$, and $\tau_{AS}{}^i$ represent the intrinsic lifetimes for A-1, A-7 and A-S recombination. As derived in the work of Beattie and Landsberg[15], the intrinsic A-1 lifetime is given by

$$\tau^i_{A1} = 3.8\times10^{-18}\cdot\frac{\left(\frac{\varepsilon_s}{\varepsilon_o}\right)^2\cdot(1+u_m)^{1/2}\cdot(1+2u_m)\cdot exp\left[\frac{(1+2u_m)E_o}{(1+u_m)k_BT}\right]}{\frac{m_e}{m_o}\cdot|F_1F_2|^2\cdot\left(\frac{k_BT}{E_o}\right)^{3/2}}, \tag{9}$$

where $u_m = m_e/m_h$ and F_1F_2 is the overlap integral of the periodic part of the electron wave function.[15,16] The intrinsic A-7 lifetime is expressed as[17,18]

$$\tau_{A7}^{i} = 2\frac{m_e E_o}{m_{eo}} \frac{\left(1-\frac{5E_o}{4k_B T}\right)}{\left(1-\frac{3E_o}{2k_B T}\right)} \tau_{A1}^{i}, \tag{10}$$

where $m_e E_o / m_{eo} \approx 3$ from Kane's nonparabolic approximation.[17] When $\Delta_o > E_o$, which is the case for InGaSb within the temperature range being considered, the A-S recombination lifetime is given by[17,18]

$$\tau_{AS}^{i} = \frac{5}{54} \frac{\varepsilon_s{}^2 m_h{}^3 m_e{}^{3/2} k_B T \Delta_o^2 (E_o + \Delta_o)}{\pi^4 \hbar^3 q^4 n_i{}^2 m_{so}^{5/2} (\Delta_o - E_o) exp\left[-\frac{(\Delta_o - E_o)}{k_B T}\right]}, \tag{11}$$

where n_i is the intrinsic carrier concentration,[26] and q is the electron charge.

2.5 Continuity equations and photocurrent densities

The distribution of minority carriers in a semiconductor material is governed by the continuity equation, which considers the drift, diffusion, photogeneration and recombination effects. At steady state under low injection conditions and no external voltage, the one dimensional (along the x axis) continuity equations for the n and p regions are:

$$D_n \frac{\partial^2 \Delta n}{\partial x^2} + G_n - \frac{\Delta n}{\tau_n} = 0, \tag{12}$$

$$D_p \frac{\partial^2 \Delta p}{\partial x^2} + G_p - \frac{\Delta p}{\tau_p} = 0, \tag{13}$$

where Δn and Δp are the excess minority carrier densities, D_n and D_p are the minority carrier diffusion coefficients, related to the carrier mobilities by Einstein's relation. The second order linear

inhomogeneous ordinary differential Eqs. (12) and (13) are solved for Δn and Δp under the following boundary conditions

$$\Delta n(x_j) = 0, \tag{14}$$

$$\left.\frac{\partial \Delta n}{\partial x}\right|_{x=0} = \frac{S_n}{D_n}\Delta n(0), \tag{15}$$

$$\Delta p(x_j + w) = 0, \tag{16}$$

$$\left.\frac{\partial \Delta p}{\partial x}\right|_{x=\infty} = 0, \tag{17}$$

In the above S_n is the surface recombination velocity of electrons, and w is the depletion region depth. The surface recombination velocity is given by[26]

$$S_n = \sigma\ v_{th,e} N_{st}, \tag{18}$$

where $v_{th,e} = \sqrt{3k_B T/m_e}$ is the electron thermal velocity and N_{st} is the number of surface trapping centers per unit area at the boundary region equal to 2.615×10^{16} m^2.[27] It should be noted that the surface recombination is not considered in eq. (17) due to the use of the ternary substrate, with relatively infinite depth (> 750 μm).

The depletion width is obtained from[26,32]

$$w = \sqrt{\left(\frac{2\varepsilon_s}{q}\right)\left(\frac{1}{N_A} + \frac{1}{N_D}\right)V_{BI}}, \tag{19}$$

where N_A and N_D are the acceptor and donor concentration and V_{BI} is the junction built-in potential given by the equation[26,32]

$$V_{BI} = \frac{k_B T}{q}\ln\left(\frac{N_A N_D}{n_i^{\,2}}\right). \tag{20}$$

Considering the diffusion lengths $L_{<n,p>} = \sqrt{D_{<n,p>}\tau_{<n,p>}}$, the general solutions of Eqs. (12) and (13) are given by

$$\Delta n = A_0\, exp\left(\frac{x}{L_n}\right) + B_0\, exp\left(-\frac{x}{L_n}\right) + C_0\, exp\left[-\alpha(\lambda,T)x\right], \tag{21}$$

$$\Delta p = C_0\left\{exp\left[-\alpha(\lambda,T)x\right] - exp\left[(x_j + w)\left(\frac{1}{L_p} - \alpha(\lambda,T)\right) - \frac{x}{L_p}\right]\right\}, \tag{22}$$

where

$$C_0 = -\frac{P_{opt}(\lambda)\cdot\left[1 - R(\lambda,T)\right]\cdot\lambda\cdot\alpha(\lambda,T)}{D_n hc\left(\alpha(\lambda,T)^2 - \frac{1}{L_n{}^2}\right)}, \tag{23}$$

$$B_0 = -\frac{C_0}{D_n}\left[1 + L_n\alpha(\lambda,T)\right]\cdot exp\left[x_j\left(\frac{1}{L_n} - \alpha(\lambda,T)\right)\right], \tag{24}$$

$$A_0 = \frac{1}{D_n - S_n L_n}\left[B_0\left(S_n L_n + D_n\right) + C_0 L_n\left(D_n\alpha(\lambda,T) + S_n\right)\right]. \tag{25}$$

Once the excess minority carriers distribution are known, the diffusion current densities in the p and n regions can be obtained using the relations

$$J_n = qD_n\left.\frac{\partial\Delta n}{\partial x}\right|_{x=x_j} \tag{26}$$

$$J_p = -qD_p\left.\frac{\partial\Delta p}{\partial x}\right|_{x=x_j+w}, \tag{27}$$

for the electron and holes respectively, while the photocurrent density in the depletion region is given by

$$J_{scr} = -q\int_{x_j}^{x_j+w} G(x)\partial x, \tag{28}$$

The total photocurrent density for the device J_{tot} is the sum of the individual contributions from each region, i.e., $J_{tot} = J_n + J_{scr} + J_p$. By definition, the responsivity, $\Re$, is then calculated from

$$\Re(\lambda, T) = \frac{J_{tot}(\lambda, T)}{P_{opt}(\lambda)}. \tag{29}$$

and therefore the quantum efficiency, η, is obtained from[26]

$$\eta = \frac{J_{tot}(\lambda, T)}{q} \cdot \frac{hc}{\lambda P_{opt}(\lambda)}. \tag{30}$$

3. RESULTS AND DISCUSSION

An $In_{0.2}Ga_{0.8}Sb$ p-n junction photodetector was formed by Zn-diffusion to an $In_{0.2}Ga_{0.8}Sb$ virtual substrate using the leaky box technique[20]. The initial substrate doping was N_D=1x10^{17} cm^{-3}. The diffusion depth was X_j=0.4 μm, with acceptor concentration of N_A= 1x10^{19} cm^{-3}. The characterization results of this device were presented elsewhere[20]. Fig. 3 shows the spectral response of a 300x300 μm^2 InGaSb photodetector compared to the model results at three different temperatures. The corresponding quantum efficiency as obtained from Eq. (4) is presented in Fig. 4. The cut-off wavelength was observed to shift to a shorter value with an increase in the responsivity and quantum efficiency when cooling the device. The shift in the cut-off wavelength is directly related to the temperature dependence of the dielectric function, through the energy band gaps, presented in both absorption and reflection coefficients. The increase in the responsivity and quantum efficiency at lower temperatures is due to the variation of minority carrier recombination. Reducing the device temperature leads to suppress thermal vibrations, resulting in increase in the minority carriers mobility and lifetime. Thus, the diffusion length increases leading to the observed increase in the performance. According to the model, for the electrons in the diffused p-region, SRH

is the dominant recombination mechanism, which has relatively lower temperature dependence. For the n-region, presented by the ternary substrate, Auger recombination dominates, especially A-S with relatively higher temperature dependence, down to approximately 180 K. Below that temperature, SRH becomes dominant.

Focusing on the room temperature spectral response (293 K), the inset of Fig. 4 shows the individual contribution from each region to the total responsivity of the device. As indicated in the figure the n region has higher influence on the performance compared to the regions at longer wavelengths. This is an advantage due to the ternary substrate compared to a binary one. The responsivity decreases at shorter wavelengths due to the domination of surface recombination. When the photon energy is less than the energy band gap, the responsivity tends to zero. For this device, this occurs at approximately 2100 nm. At lower photon energies, most carriers are generated in the n region since the absorption length is longer. As the photon energy increases, the absorption length is reduced and the responsivity of the p region becomes dominant. This occurs at a wavelength of 1100 nm for this device. Focusing on this fact, Fig. 5 presents the effect of the Zn-diffusion depth, x_j, on the quantum efficiency. At shorter wavelength, increasing the diffusion depth (the p-region depth) increases the recombination probability of photogenerated carriers, thus reducing the quantum efficiency.

The effect of Zn-diffusion depth and temperature on responsivity is future discussed in the inset of Fig. 5, assuming an arbitrary wavelength of 1.9 μm. As the diffusion depth increases, fewer photogenerated carriers from the p-region reach the depletion layer, thereby reducing the responsivity. At a given temperature, if the length is shorter than a certain value (optimum diffusion depth), the responsivity decreases because fewer photons can get absorbed in such a narrow p-

region. The optimum diffusion depth has been found to decrease with cooling of the device, with a value of 0.3 μm at 293 K.

The responsivity for various acceptor and donor concentrations for the same $In_{0.2}Ga_{0.8}Sb$ photodetector is shown in Fig. 6. Increasing the concentration of acceptors and/or donors slightly augments the built-in potential that serves to separate the generated electron-hole pairs (Eq. 20). However, the overall effect is a decrease in the depletion region width, where the photogeneration of carriers mainly takes place (Eq. 19). Thus, higher doping levels adversely affect responsivity, as can be seen in the figure. On the other hand, very low doping levels are not practically achievable besides it deteriorates the transient response.

4. CONCLUSIONS

The spectral response of $In_{0.2}Ga_{0.8}Sb$ p-n junction infrared photododetectors has been analyzed using a theoretical model based on the continuity equations of the minority carriers in the p, n and space charge regions. The absorption coefficient and normal-incidence reflectivity have been incorporated using a dielectric function model developed by Adachi and extended here to account for temperature effects. The carrier mobility has been calculated using the temperature-extended Caughey-Thomas model. The changes in the absorption coefficient and reflectivity with decreasing temperature cause a shift in the cutoff wavelength to shorter values while the Auger recombination mechanism have proven to have a dominating effect in the horizontal shift of the spectral response with cooling. These effects correspond to the energy bands variation with temperature, which has been approximated using Varshini's equation. The effects on the spectral response due to the variation of temperature, photon energy, diffusion depth, and carrier

concentration have all been analyzed. By appropriate combination of the aforementioned parameters, the performance of the device can be optimized.

5. ACKNOWLEDGEMENT

This work is supported by Breakthrough Atmospheric Remote Sensing Program under NASA's Earth Science Technology Office and NASA's Enabling Concepts & Technologies Program. The authors acknowledge Ishwara Bhat and Chris Moore for their constant support.

References

1. P. S. Dutta and H. L. Bhat, "The physics and technology of gallium antimonide: an emerging aptoelectronic material", J. Appl. Phys. **81**(9), 5821-5870 (1997).
2. T. Refaat, N. Abedin, I. Bhat, P. Dutta, and U. Singh, "Characterization of InGaSb/GaSb p-n photodetectors in the 1.0- to 2.4-μm wavelength range", Opt. Eng. **43**(5), 1014-1015 (2004).
3. P. S. Dutta and T. R. Miller, Journal of Electronic Materials **29**, 956 (2000).
4. S. Adachi, "Model dielectric constants of GaP, GaAs, GaSb, InP, InAs, and InSb", Phys. Rev. B **35**(14), 7454-7463 (1987).
5. S. Adachi, "Optical dispersion relations for GaP, GaAs, GaSb, InP, InAs, InSb, $Al_xGa_{1-x}As$, and $In_{1-x}Ga_xAs_yP_{1-y}$",J. Appl. Phys. **66**(12), 6030-60-40 (1989).
6. S. Adachi, "Excitonic effects in the optical spectrum of GaAs", Phys. Rev. B **41**(2), 1003-1013 (1990).
7. S. Adachi, "Effects of the indirect transitions on optical dispersion relations", Phys. Rev. B **41**(6), 3504-3508 (1990).
8. S. Adachi, *Physical properties of III-V semiconductor compounds*, (Wiley, New York, 1992).
9. D. M. Caughey and R. E. Thomas, Proc. IEEE **55**, 2192 (1967).
10. M. Sotoodeh, A. H. Khalid, and A. A. Rezazadeh, "Empirical low-field mobility model for III-V compounds applicable in device simulation codes", J. Appl. Phys. **87**(6), 2890-2900 (2000).
11. D. Martín and C. Algora, "Temperature-dependent GaSb material parameters for reliable thermophotovoltaic cell modelling", Semicond. Sci. Technol. **19**, 1040-1052 (2004).
12. R. N. Hall, "Electron-Hole recombination in germanium", Phys. Rev. **87**, 387 (1952).
13. W. Shockley and W. T. Read, "Statistics of the recombination of holes and electrons", Phys. Rev. **87**(5), 835-842 (1952).

14. T. H. Gfroerer, L. P Priestley, M. F. Fairley, and M. W. Wanlass, "Temperature dependence of nonradiative recombination in low-band gap $In_xGa_{1-x}As/InAs_yP_{1-y}$ double heterostructures grown on InP substrates", J. Appl. Phys. **94**(3), 1738-1743 (2003).

15. A. R. Beattie and P. T. Landsberg, "Auger effect in semiconductors", Proc. R. Soc. A **249**(1256), 16-29 (1959).

16. M. G. Burt and C. Smith, "Overlap integrals for Auger recombination in direct gap III-V semiconductors", J. Phys. C: Solid State Phys. **17**, L47-L52 (1984).

17. A. Rogalski, R. Ciupa and W. Larkowski, "Near room-temperature InAsSb photodiodes: Theoretical predictions and experimental data", Solid State Electron. **39**(11), 1593-1600 (1996).

18. Y. Tian, T. Zhou, B. Zhang, H. Jiang and Y. Jin, "The effect of Auger mechanism on n+-p GaInAgSb infrared photovoltaic detectors", IEEE Trans. on Elect. Dev., **6**(4), 656-660 (1999).

19. P. C. Findlay, C. R. Pidgeon, H. Pellemans, R. Kotitschke, B. N. Murdin, T. Ashley, A. D. Johnson, A. M. White, and C. T. Elliott, "Auger recombination dynamics of $In_xGa_{1-x}Sb$", Semicond. Sci. Tehnol. **14**, 1026-1030 (1999).

20. T. F. Refaat, M. N. Abedin, V. Bhagwat, I. B. Bhat, P. S. Dutta and U.N. Singh, "InGaSb photodetectors using an InGaSb substrate for 2 μm applications", Appl. Phys. Lett. **85**(11), 1874-1876 (2004).

21. R. Rousina, C. Halpin, and J.B. Webb, "Growth and characterization of $In_{1-x}Ga_xSb$ by metalorganic magnetron sputtering", J. Appl. Phys. **68**(5), 2181-2186 (1990).

22. Y. P. Varshni, "Temperature dependence of the energy gap in semiconductors", Physica **34**, 149-154 (1967).

23. Ioffe Physico-Technical Institute's electronic archive on Semiconductor Materials, http://www.ioffe.rssi.ru/SVA/NSM/, last accessed 9/12/2004.

24. S. Logothetidis, L. Viña, and M. Cardona, "Temperature dependence of the dielectric function and the interband critical points of InSb", Physical Review B **31**(2), 947-957 (1985).

25. S. Zollner, M. Garriga, J. Humlicek, S. Gopalan, and M. Cardona, "Temperature dependence of the dielectric function and the interband critical-point parameters of GaSb", Phys. Rev. B **43**(5), 4349-4360 (1991).

26. S.M. Sze, *Physics of semiconductor devices*, 2nd ed. (Wiley, New York, 1999).

27. A.S. Sedra and K.C. Smith, *Microelectronic Circuits*, 4th ed. (Oxford Press, New York, 1982).

28. M. Zierak, J. M. Borrego, I. Bhat, R. J. Gutmann, and G. Charache, AIP Conf. Proc. **401**, 55 (1997).

29. R Wiersma, J. Stotz, O. Pitts, C. Wang, M. Thewalt and S. Watkins, "Electrical and optical properties of carbon-doped GaSb", Phys. Rev. B **67**, 165202 (2003).

30. P.S. Dutta, V. Prasad and H.L. Bhat, "Carrier compensation and scattering mechanisms in p-GaSb", J. Appl. Phys. **80**(5), 2847-2853 (1996).

31. D.L. Rode, "Electron mobility in direct-gap polar semiconductors", Phys. Rev. B **2**(4), 1012-1024 (1970).

32. G. Charache, P. Baldasaro, L. Danielson, D. DePoy, M. Freeman, *et. al.*, "InGaAsSb thermophotovoltaic diode: Physics evaluation", J. Appl. Phys. **85**(4), 2247-2252 (1999).

33. K. Beyzavi, K. Lee, D. M. Kim, and M. I. Nathan, "Temperature dependence of minority-carrier mobility and recombination time in p-type GaAs", Appl. Phys. Lett. **58**(12), 1268-1270 (1991).

Table I. Temperature dependence of the critical-point energies of GaSb and InSb, with parameters used in Varshni's equation for each energy level (after Refs. 23-25).

Critical Point Energies	GaSb			InSb		
	$E(0)$ (eV)	δ (x10^{-4} eV.K^{-1})	β (K)	$E(0)$ (eV)	δ (x10^{-4} eV.K^{-1})	β (K)
E_o	0.812	4.2	140	0.24	6	500
$E_o+\Delta_o$	1.6	5	143	1.2	6	500
E_1	2.186	6.8	147	2	6.84	132
$E_1+\Delta_1$	2.621	6.7	176	2.49	6.46	170
E_2	4.32	9	376	4.24	5.4	0

Table II. Parameters used in the temperature extended Caughey-Thomas model for calculating the electron (e) and hole (h) mobilities for GaSb (Ref. 11) and InSb (Ref. 27).

	Material/Carrier			
Parameters	GaSb/e	GaSb/h	InSb/e	InSb/h
μ_{max} (cm^2/V-s)	5650	875	7.8×10^4	750
μ_{min} (cm^2/V-s)	1050	190	5000	100
N_{ref} (cm^{-3})	2.8×10^{17}	9×10^{17}	7×10^{16}	6×10^{17}
ϕ	1.05	0.65	0.7	0.6
θ_1	2.0	1.7	...	...
θ_2	2.8	2.7	...	...

List of Figure Captions

FIG. 1 Schematic cross section of the modeled $In_{1-\chi}Ga_{\chi}Sb$ p-n photodetector. x_j is the Zn-diffusion depth and w is the depletion region width.

FIG. 2 $In_{0.2}Ga_{0.8}Sb$ absorption coefficient and normal-incidence reflection coefficient versus wavelength calculated at temperatures of 253, 273 and 293 K.

FIG. 3 Spectral response at different temperatures obtained from the model compared to the experimental data. The model results were obtained assuming diffusion depth x_j = 0.4 μm, and acceptor and donor concentrations of $N_A = 1x10^{19}$ cm^{-3} and $N_D = 1x10^{17}$ cm^{-3}, respectively.

FIG. 4 Calculated quantum efficiency variation with wavelength at different temperatures. The results obtained using the same parameters of Fig.3. The inset shows the 293 K calculated responsivity of the different regions of the device compared to the total responsivity.

FIG. 5 The calculated variation of the quantum efficiency with the Zn-diffusion depth, obtained at 293 K. Focusing on 1.9 μm wavelength, the inset shows the responsivity variation with the Zn-diffusion depth at three different temperatures.

FIG. 6 Responsivity variation with Zn-diffusion concentration (acceptor level N_A) and the original doping of the ternary substrate (donor level N_D). Calculations assume 0.8 composition, 293 K temperature, 0.4 μm Zn-diffusion depth and 1.9 μm wavelength of the incident radiation.

FIG 1

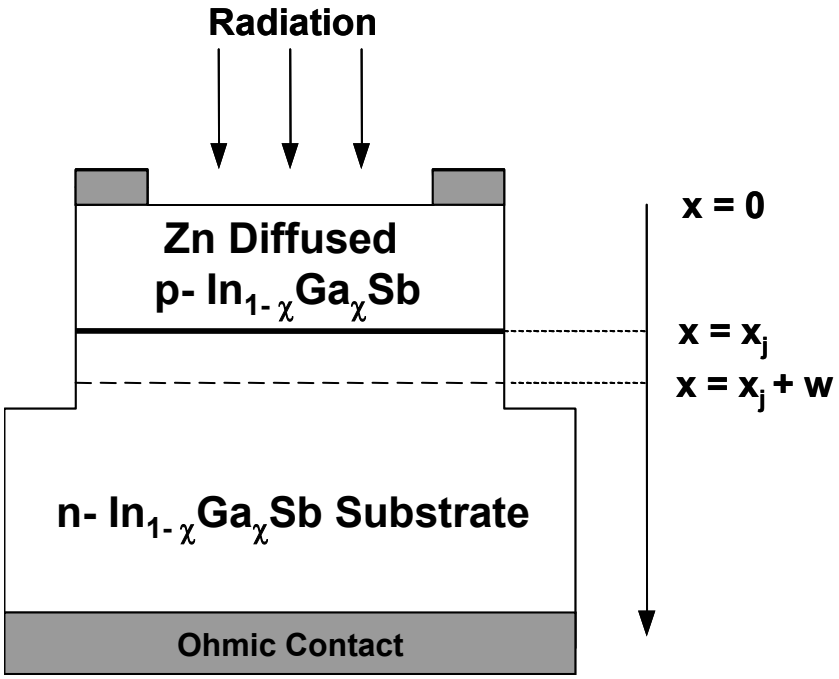
Radiation
Zn Diffused
p- In1-χGaχSb
x = 0
x = xj
x = xj + w
n- In1-χGaχSb Substrate
Ohmic Contact

FIG 2

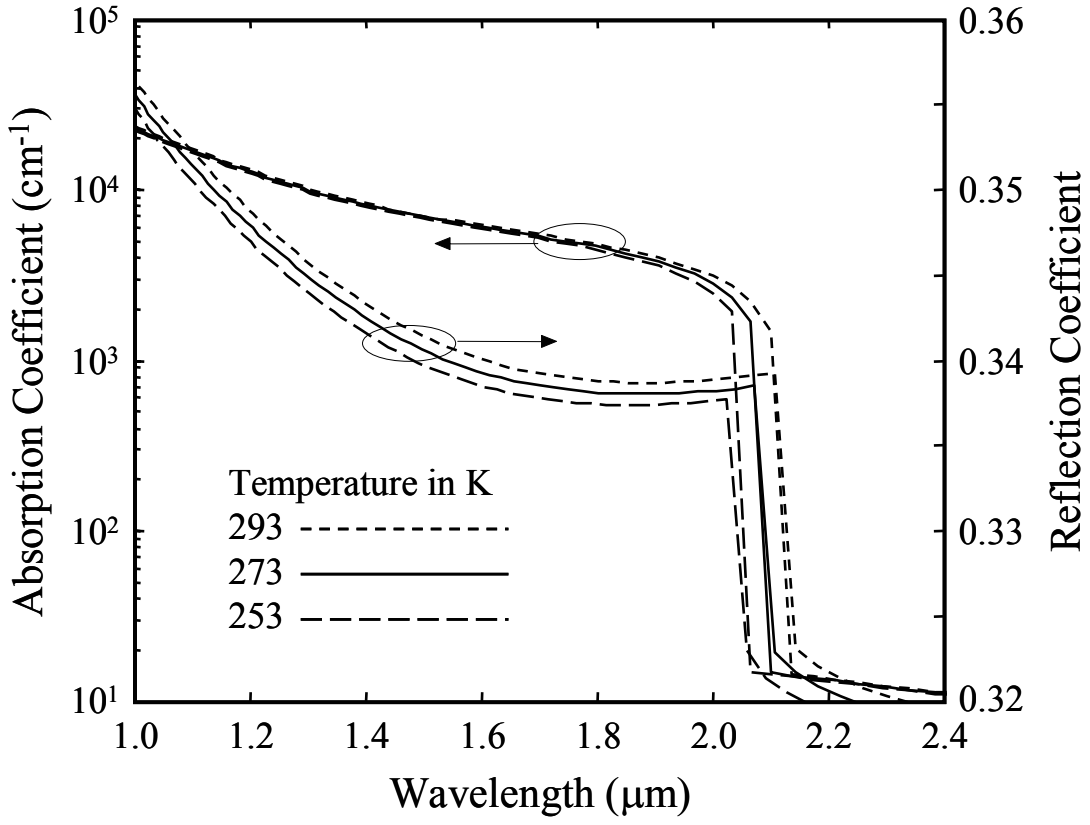
Absorption Coefficient (cm-1)
Reflection Coefficient
Wavelength (μm)
Temperature in K
293
273
253
10^5
10^4
10^3
10^2
10^1
0.36
0.35
0.34
0.33
0.32
1.0
1.2
1.4
1.6
1.8
2.0
2.2
2.4

FIG 3

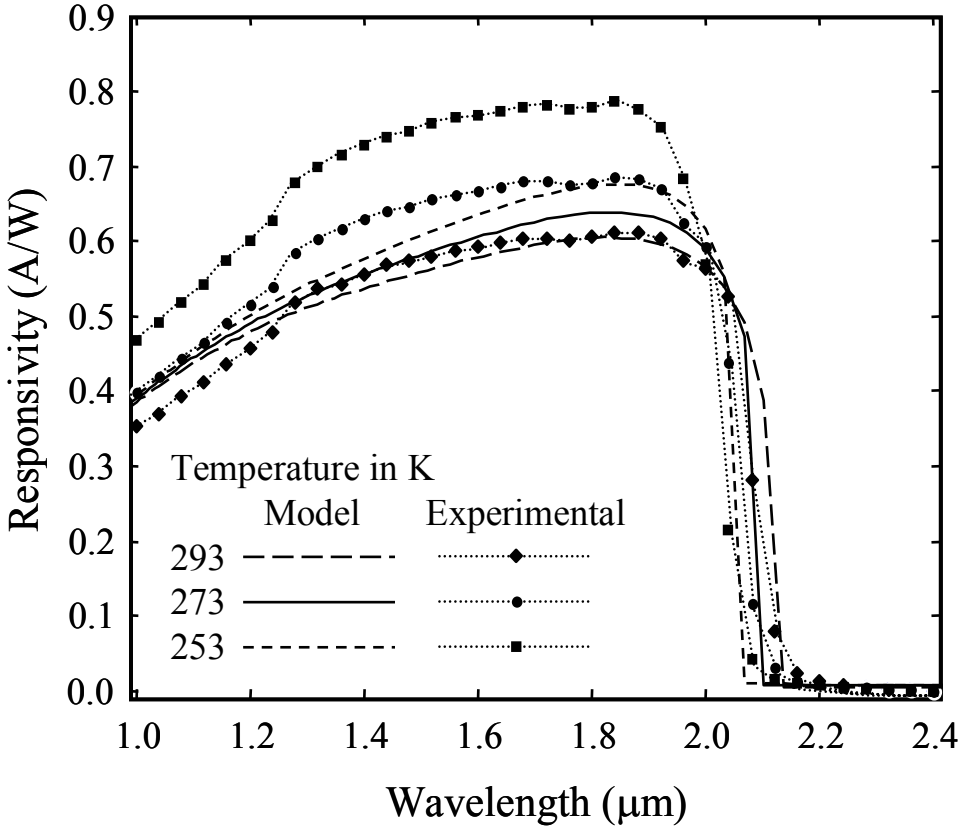
Responsivity (A/W)
0.9
0.8
0.7
0.6
0.5
0.4
0.3
0.2
0.1
0.0
1.0
1.2
1.4
1.6
1.8
2.0
2.2
2.4
Wavelength (μm)
Temperature in K
Model
Experimental
293
273
253

FIG 4

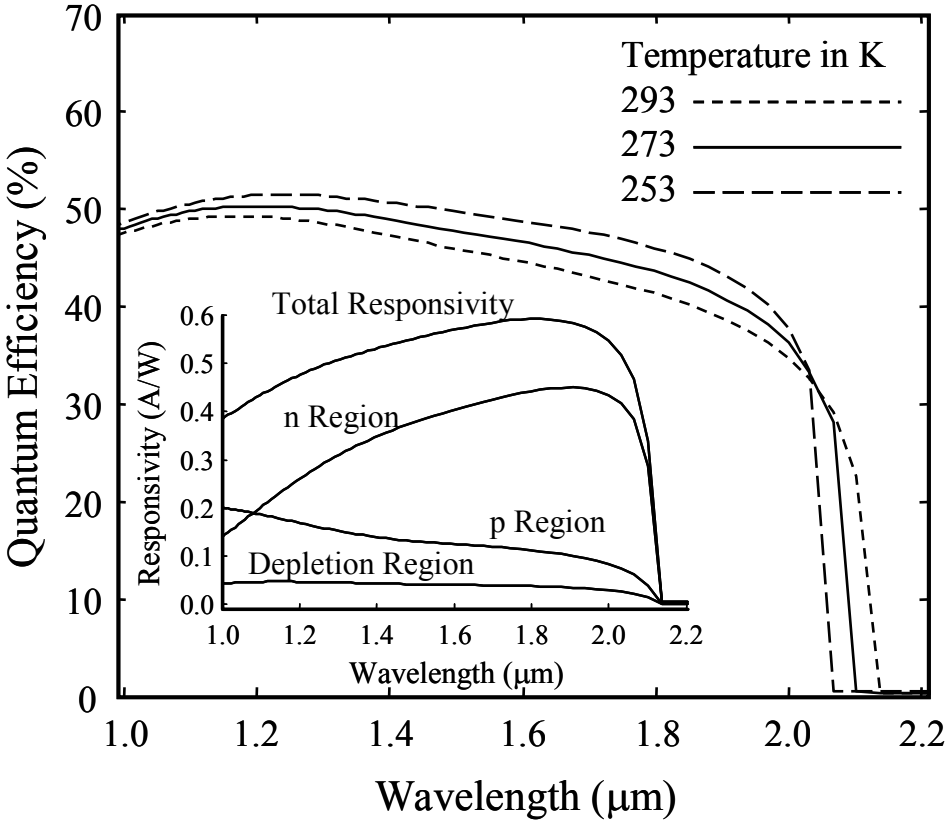
Temperature in K
293
273
253
Quantum Efficiency (%)
Wavelength (μm)
Total Responsivity
n Region
p Region
Depletion Region
Responsivity (A/W)
Wavelength (μm)

FIG 5

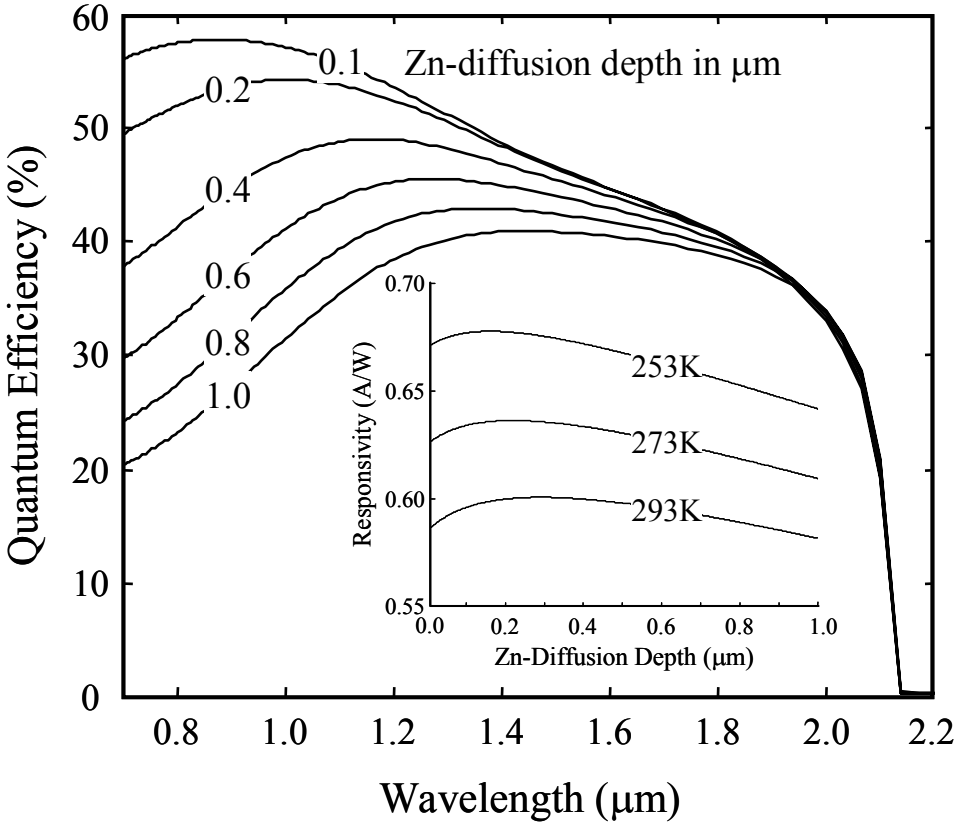
Quantum Efficiency (%)
Wavelength (μm)
Zn-diffusion depth in μm
0.1
0.2
0.4
0.6
0.8
1.0
Responsivity (A/W)
253K
273K
293K
Zn-Diffusion Depth (μm)

FIG 6

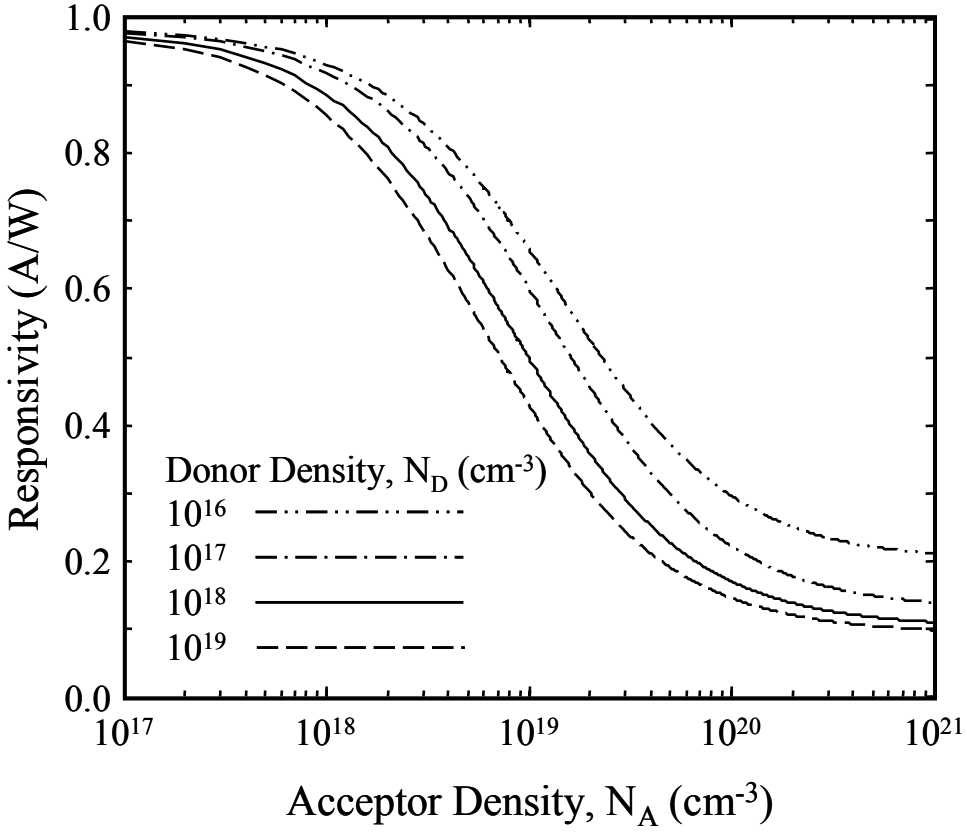
1.0
0.8
0.6
0.4
0.2
0.0
Responsivity (A/W)
Donor Density, N_D (cm^{-3})
10^{16}
10^{17}
10^{18}
10^{19}
10^{17}
10^{18}
10^{19}
10^{20}
10^{21}
Acceptor Density, N_A (cm^{-3})